THE INTERNATIONAL JOURNAL OF MEDICAL ROBOTICS AND COMPUTER ASSISTED SURGERY
Int J Med Robotics Comput Assist Surg 2009; **5**: 267–275.
Published online 28 April 2009 in Wiley InterScience (www.interscience.wiley.com). **DOI:** 10.1002/rcs.257

ORIGINAL ARTICLE

Optimized port placement for *in vivo* biosensors

Brady W. King[1]*
Luke A. Reisner[1]
R. Darin Ellis[2]
Michael D. Klein[3]
Gregory W. Auner[1] and
Abhilash K. Pandya[1]

[1]*Department of Electrical and Computer Engineering, Wayne State University, Detroit, MI, USA*

[2]*Department of Industrial and Manufacturing Engineering, Wayne State University, Detroit, MI, USA*

[3]*Department of Pediatric Surgery, Children's Hospital of Michigan, Detroit, MI, USA*

*Correspondence to: Brady W. King, 5050 Anthony Wayne Drive, #3157, Detroit, MI 48202, USA.
E-mail: bwking@wayne.edu

Accepted: 7 March 2009

Abstract

Background We discuss the implementation of an automated port placement system for use with laparoscopic *in vivo* biosensors. Biosensors have physical limitations that make port placement crucial to proper data collection. The port placement process is prohibitively complex to execute optimally by human estimation.

Methods Port placement algorithms were integrated into an image-guided surgery system. Variables for optimization of ports include biosensor length, data collection restrictions, obstacles, and regions of interest. The port placement is applied to 3D virtual 'patients' created from medical imaging data. An example implementation for a Raman biosensor probe was created.

Results The prototype system can correctly find ideal port locations on a virtual patient based on biosensor limitations and regions of interest. Conversely, the system can evaluate and score an individual port selected by a user.

Conclusion As biosensors become incorporated into laparoscopic surgical environments, an automated port placement system would enable their optimized integration. Copyright © 2009 John Wiley & Sons, Ltd.

Keywords port placement; sensor integration; image-guided surgery; Raman spectroscopy; medical robotics; virtual reality

Introduction

Robotic surgery is increasingly being used in medical procedures (1). For example, laparoscopic robots such as the da Vinci® (Intuitive Surgical, Sunnyvale, CA, USA) are finding more common use because they provide advantages such as tremor filtration and motion scaling (2). These robots operate through small incisions in the patient's skin, making robotic surgery less invasive than open surgery. Another field of technology beginning to be applied to medical care consists of biological sensors (biosensors), which are capable of gathering many types of data (3–6). For example, biosensors based on Raman spectroscopy (a light-based sensing technique) have been shown to be effective at identifying various forms of cancer (7–10). Combining the stability and positioning abilities of medical robots with the detection capabilities of biosensors would allow surgeons to more accurately pinpoint and treat diseases (11–13).

The first step in utilizing a biosensor *in vivo* is to identify a suitable port of entry into the body. In this paper, a novel technique is presented for automated port placement for a biosensor with stringent physical requirements. It addresses restrictions in biosensor probe placement, such as incident angle, as well as inadequacies of existing port placement solutions. The technique

allows the surgeon to select a region of tissue within the patient's body that he/she wishes to scan, and an optimized port location is computed for that region. The algorithm avoids unsafe port locations that would lead to collisions between the probe and anatomical structures. It also maximizes the performance of the biosensor by allowing proper orientation of the probe at the target location. Optimized port placement minimizes the risk to the patient while ensuring the most effective use of biosensor technology. This will enable a surgeon to make more informed and timely decisions during interventions.

Biosensors

Many of the most effective biosensor technologies (Raman spectroscopy, surface acoustic wave, glucose monitoring, etc.) require close proximity or direct contact with tissue in order to collect optimal data. Biosensors may also scan a localized region, requiring the sensor to be placed in multiple positions within a volume of interest. Furthermore, the angle between the probe and the tissue may be important, resulting in limited effectiveness when outside some operating envelope. For example, Figure 1 shows that Raman data collected at a 45° angle has a weaker signal than data collected from an orthogonal placement. For spectroscopic sensors, the maximum performance is typically attained when the probe is perpendicular to the tissue (5). In addition, the size and degrees of freedom of the probe can make it difficult to achieve optimal sensor positioning. The complexity of tissue surfaces and the presence of obstructions inside the body also contribute to the difficulty.

In minimally invasive medical procedures, surgeons operate through small ports in the patient's skin. Thus, any biosensor that is used during these procedures must be inserted and used through one of these ports. The biosensor must therefore pivot at a single location on the skin surface, severely limiting the positions and orientations that it can reach. Consequently, the choice of a port's location is critical to the performance of a biosensor.

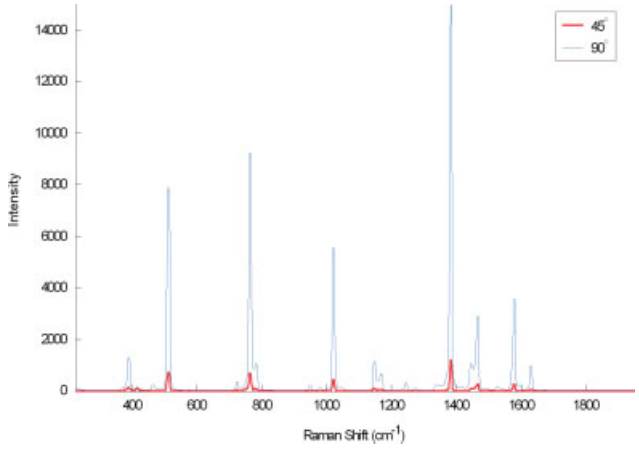

Figure 1. Raman spectra of naphthalene captured with a Raman probe at angles of 45° and 90° (perpendicular)

Port placement

An automated port placement algorithm can be used to help select an optimal location through which a probe can be threaded into the body. Some automated techniques for port placement have been developed (14–20). In general, these techniques were designed to place two surgical instruments and a camera for laparoscopic procedures in a manner that makes the surgeon more comfortable while ensuring better accessibility to the surgical site. Unfortunately, these techniques do not address the needs of optimal biosensor placement.

Many of the techniques place the surgical instruments in a 'golden triangle' arrangement. In this arrangement, the camera port is placed on the top of the triangle with the two surgical arm ports on either side. For biosensor placement, only a single port is required. Moreover, the goal of biosensor placement is to maximize the surface area that can be scanned or to achieve the highest quality reading, depending on the type of sensor. Thus, the golden triangle is not applicable for optimal biosensor placement. However, the golden triangle can still be used to place the endoscope and surgical tools as needed. While this work does not take into account other tools within the surgical site at the time of biosensor placement, it would be possible to consider the other tools in the collision avoidance algorithms discussed later in this paper.

Evaluating the performance of the biosensor's port placement requires different metrics than the existing port placement techniques. Many of the existing port placement techniques focus on a specific surgical procedure (e.g. coronary artery bypass) and use its outcome as a measure of the performance. In contrast, the evaluation of biosensor placement must focus on the ability to achieve high quality scans of target areas. The use of a biosensor is a preamble to the actual surgical procedure (resection) and its outcome. Thus, the area of coverage and probability of successful scans are better metrics for a biosensor application.

The technique outlined in this paper addresses the aforementioned restrictions in biosensor probe placement as well as the inadequacies of existing port placement solutions. Our technique maximizes a probe's ability to reach many small, specific targets from one port location. By taking into account the physical limitations of a biosensor and obstructions within the scanning volume, we can ensure the most effective coverage of a target region.

Materials and Methods

The goal of this work was to create an optimized port placement system for use with biosensor-enhanced minimally invasive surgery. To implement such a system, two computer algorithms were designed. One algorithm was used to determine points that were reachable from a given port location, and another was used to determine

DOI: 10.1002/rcs

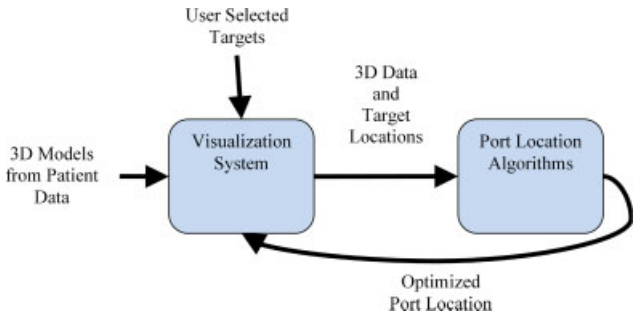

Figure 2. Data flow within the system

an optimal port location. A visualization interface was also created to allow easier use of the system and interpretation of its results.

From a user's perspective, the system was designed to operate in the following manner. First, 3D models of a patient must be created (via segmentation) from medical imaging, e.g. CT or MRI scans. Next, areas of interest (biosensor scan locations) are chosen on the 3D models. The system then determines an optimized port location based on the 3D information and the limitations of the biosensor (Figure 2). Alternatively, the surgeon may select a port location, and the system determines all possible valid targets. This information is presented to the user in a virtual reality interface.

Raman biosensor

To prove the feasibility of the system, the implementation was designed around a specific Raman spectroscopy probe (Process RamanProbe, InPhotonics, Norwood, MA, USA). However, the system was intended to generalize to other types of biosensors. There are parameters and functions that can be changed in our algorithms to accommodate biosensors of different designs, such as probes of different dimensions or having angle-dependent response functions.

The Raman probe used in the design and validation of the system was an inflexible cylinder, 20 cm in length and 1 cm in diameter (Figure 3). Like most optical sensors, the probe achieves the best scan when it is placed perpendicular to the tissue of interest. Additional biosensor components are housed in an external box attached to the probe through a cable. A Raman probe was chosen because it has been shown to enable *in vivo* cancer detection (21–23).

3D models

The algorithms detailed in this paper are designed to work with three-dimensional (3D) representations of patient data. These 3D models are made up of triangles, which are themselves defined by points. Each point in a 3D model has a corresponding normal vector that indicates a direction approximately perpendicular to the surface at that point (the normal vector for each point is the

Figure 3. Raman spectroscopy probe

average of the normal vectors for all triangles that share the point). Each point in the model can be considered a possible point for biosensor data capture, referred to as a target point. Therefore, if a model has less detail (points), the algorithms will execute faster, but there will be a reduced number of targets a surgeon can choose to scan. The port placement system supports whatever level of model detail is required by the surgical application. If the provided models lack sufficient detail, a pre-processing stage can be used to increase the number of points.

A special 'skin' model, which contains all potential port locations, must be defined. This model is thin (i.e. just the surface of the patient's skin and not its thickness), which aids the collision detection algorithm (described in the following section). Each point in the skin model can be a possible port location. Thus, the model should be as detailed as necessary for the surgical application.

Reachable point algorithm

An algorithm was created to test whether a point is reachable from a given port location (Figure 5). The algorithm tests three criteria to determine if a point is reachable. If a point fails any test, it is determined to be unreachable. Thus, it is not subjected to any further tests, which shortens the execution time of the system. The three tests are described in the following subsections.

Biosensor length test

The first test is a simple biosensor length test, which ensures the biosensor is long enough to reach the target from the port location. If the target point is farther from a port location than the length of the biosensor, it is considered to be unreachable. This test is performed first because it is computationally the fastest and eliminates many unreachable targets.

Collision test

The second test is a collision algorithm that ensures that the biosensor does not collide with any other point while moving the probe towards the given target. The algorithm was designed to be extremely fast for the port placement application with a rigid probe. To handle a biosensor probe with a flexible or multi-jointed design, the algorithm could be modified. Because every point on every model is considered a potential collision, any surface that is deemed to be non-obstructing should not be included in the 3D scene representation of the patient.

The first step of the collision test is to create a vector from the given port location point to the target point. In addition, vectors from the port location to all other geometry points (potential points of collision) are created (Figure 4).

The second step is to determine the distance from the port location to each of the potential points of collision. Any point that is farther away than the target point is eliminated as a point of collision, as the biosensor will never have to reach far enough to intersect with that point.

Any remaining potential collision points are now determined to be closer to the port location than the target point. The third and final step determines whether any of these points are within the radius of the biosensor. If the distance (equation 1) between a potential collision point and the vector between the port location and the target point (representing the biosensor) is less than the radius of the biosensor, then the biosensor would collide with that point while trying to reach the target point. If even a single collision is determined to occur, the target point is deemed unreachable:

$$x = ||\mathbf{v}_2|| \sin(\arccos(\hat{\mathbf{v}}_1 \bullet \hat{\mathbf{v}}_2)) \quad (1)$$

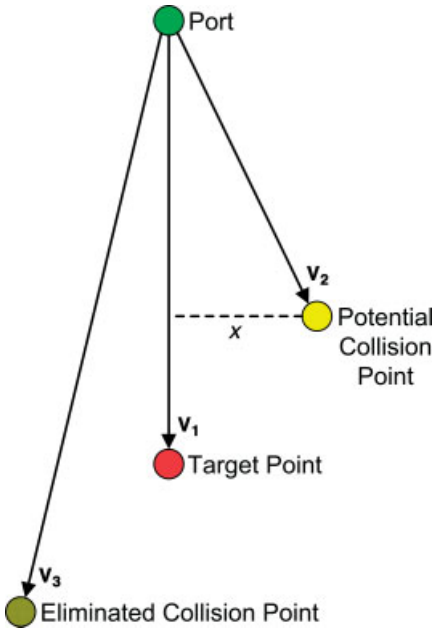

Figure 4. Diagram of the collision test algorithm. A collision occurs when $||\mathbf{v}_2|| < ||\mathbf{v}_1||$ and $x <$ radius of biosensor

Biosensor-specific scoring function

The final test is a biosensor-specific scoring function. This test is used to determine the quality of a scan the biosensor will obtain from a given target. A score of 0 is treated as a non-reachable point, while a score of 1 is considered a perfect scan. For our Raman probe, we used a relatively simple scoring function (equation 2):

$$\text{Score} = \begin{cases} 1 - \dfrac{90^\circ - \theta}{45^\circ} & 45^\circ \le \theta \le 90^\circ \\ 0 & \text{Otherwise} \end{cases} \quad (2)$$

In equation 2, θ represents the minimum angular deviation of the probe from the tissue surface. The equation produces a 1 for a perfectly perpendicular orientation ($\theta = 90^\circ$ from the surface) and decreases linearly to 0 as the probe approaches 45° from perpendicular. Although Raman biosensors are known to have non-linear response functions (5), this linear equation reasonably approximates the same response. It was chosen for its simplicity and to illustrate the functionality of the port placement algorithm (detailed below). Non-linear functions or functions with angles other than 45° could be used to accommodate other biosensor probes.

Identifying the best port location

The best port location is one that enables the best coverage of the target area by the biosensor. To find this location, the system evaluates each point in the skin model (or a user-selected subset of the skin) for its suitability as a port location (Figure 6). The evaluation of each skin point is carried out by executing the reachable point algorithm with the skin point and all target points. This process provides the number or percentage of reachable target points and the average biosensor-specific score for each potential port location.

For the test application (Raman cancer detection), priority is given to the number of reachable points rather than to the biosensor-specific scoring function when determining the best port location. This is because it is critical to ensure that as many reachable points as possible are scanned, due to the importance of not missing any cancerous cells during resection. Therefore, the best port location enables the maximum number of target points to be reached. If two or more port locations allow the same number of target points to be reached, the best port is chosen using the average result of the biosensor-specific scoring function. For example, if two ports can reach the same number of target points with a Raman biosensor, the port location that provides the smallest average angular deviation from perpendicular will be chosen.

It is possible that other biosensors may require different priorities for the scoring function and the number/percentage of reachable points. In this case, a weighted decision function could be utilized, allowing a combination of the number of reachable points and the scoring function to be used to determine which port is best.

DOI: 10.1002/rcs

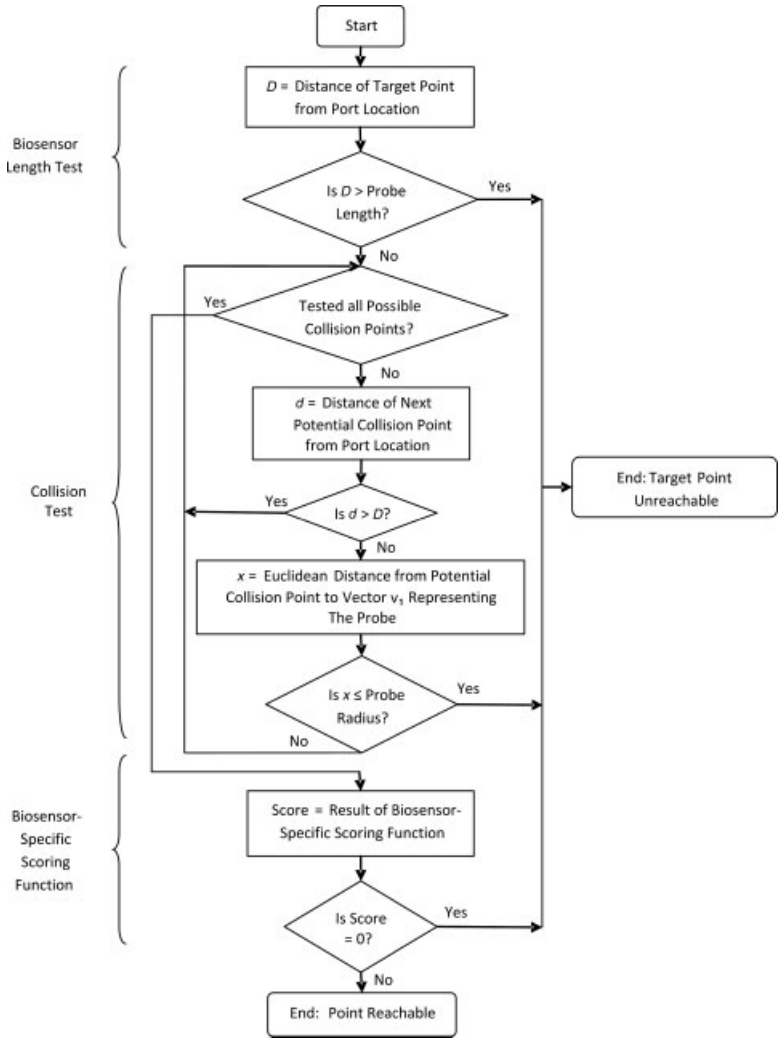

Figure 5. Flowchart of the reachable point algorithm

Visualization

A 3D virtual reality display is used for the interface of the port placement system. It is based on 3D Slicer (24), an open source application for visualizing medical data. 3D Slicer displays the 3D models derived from segmentation as well as the various interface elements used by the system. To accommodate the graphics and interactivity needed for the port placement application, a custom module was added to 3D Slicer. The module handles target area selection, port placement, and the presentation of the system's results.

Target area selection is carried out in the following fashion. First, the user selects a point in the centre of a volume he/she wishes to scan, causing a 'volume of interest' box to appear around that point. Then the user adjusts the size of the box to enclose the desired target surface area. Once the region is finalized, small markers appear at each of the points within the region (Figure 7). These points are considered to be the target points.

Once the target points have been selected, the system can find an optimized port location. It can evaluate every point on the skin model, or the search can be restricted to a subset of the skin model. Selecting a subset of the skin model is accomplished in exactly the same fashion as choosing target points, consisting of a box being placed and its size adjusted. The chosen subset of points is also highlighted with markers (of a different color than the targets).

After the port placement algorithms are executed, a marker is placed at the optimized port location. This enables the user to see the port location relative to other body structures. In addition, a pop-up box displays the percentage of reachable points and the average biosensor-specific score for that location.

In addition to the computer-generated optimal port location, the user can choose a specific port location for the system to evaluate. This simply requires the user to click at a desired location on the skin model. If target points have been selected, the percentage of reachable points and the average biosensor-specific score for the chosen port are calculated and presented. If a target region has not been selected, the system calculates all reachable points (points that pass all three tests within the reachable point algorithm) from the chosen port.

DOI: 10.1002/rcs

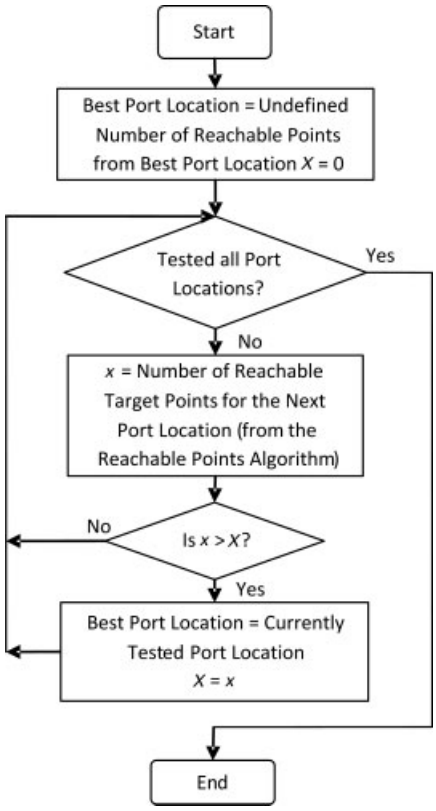

Figure 6. Flowchart for the selection of the best possible port location. This method is optimized for cancer detection using Raman spectroscopy (maximizing the number of reachable points). Other methods can be utilized as necessary

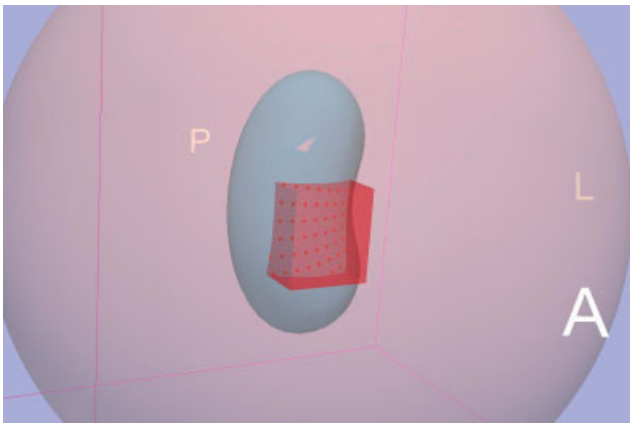

Figure 7. Target volume selection (red box) within the visualization system

These points are highlighted with markers on the 3D models.

Results

To verify the operation of the port placement system, a number of test scenes were created. These scenes contained simple objects (planes, cylinders, etc.) with geometrically provable solutions for the optimal port locations. Using these scenes, the various components of the system were validated. It was shown that the algorithms were able to find optimal port locations, find all reachable target locations, and avoid collisions. Figure 8 demonstrates the test scenarios that were used to validate the system.

Figure 8a shows a cross-section of two parallel planes. The top plane represents the skin surface, whose points are potential port locations. The bottom plane is identical to the top plane but shifted downwards. It represents a target surface, whose points must be reached by the biosensor. In this scenario, the algorithms were executed with a single point selected at a time as the target. From the diagram, it is clear that the skin point directly above each target point is the best location for a port. This is because the approach vector from the skin surface to the target point is perpendicular to the target surface, which maximizes the Raman scoring function. This scenario was designed to verify that the system would function properly under very simple conditions.

The test scenario in Figure 8b is very similar to the one in Figure 8a. The only difference is that the algorithms were executed with multiple points selected at a time as the targets. The selected target points were always odd in quantity, centred below one of the skin points, and uniformly spaced. Under these constraints, the best port location is the skin point above the centre of the group of target points. For any other skin point, the average value of the biosensor scoring function is lower because the average angle from the approach vector to the target surface at each target point is further from perpendicular. The purpose of this scenario was to validate the system's operation when multiple target points are selected.

Figure 8c shows a cross-section of two concentric cylinders. The outer cylinder represents the skin surface, and the inner cylinder represents the target surface. The cylinders are made from the same model with the same points, but they were scaled to different radii. The algorithms were executed with a single point selected at a time as the target. As in the test scenario in Figure 8a, the best port location for each target point is the skin point directly across from it. This test was used to verify that the system would work with non-planar (curved) surfaces.

In Figure 8d, there is another cross-section of two planes. The top and bottom planes represent the skin and target surfaces, respectively. In this scenario, the algorithms were executed with a single point selected at a time as the target. Because of the angle between the two planes (45°), the best port location for a given target point is not directly above the target point. Instead, the best port location, which maximizes the biosensor scoring function, is more to the right of the target point. This is because the approach vector and target surface at the target point are perpendicular for the skin point on the right. However, there is an exception for the rightmost target point. The distance from this point to the green triangle point on the skin surface was made to be greater than the length of the biosensor probe. Thus, the green triangle point was not a valid port location. The blue circle point of the skin surface enables the biosensor probe to reach the target

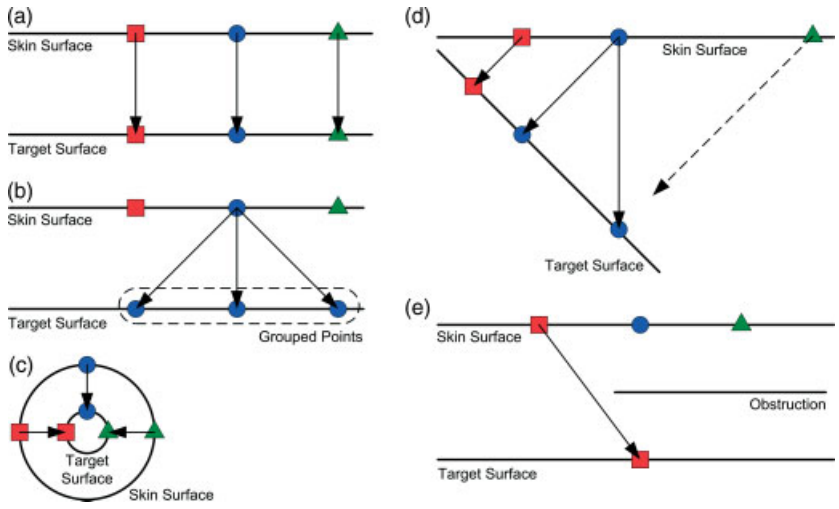

Figure 8. Cross-sectional views of five test scenarios used to validate the performance of the system

and achieves an angle closest to perpendicular, so it is the best port location. Therefore, this test scenario verifies the system's performance when the skin and target surfaces are not parallel and when a target point exceeds the length of the biosensor probe.

Figure 8e shows a test scenario that is very similar to the one in Figure 8a. The same parallel skin and target surfaces are used, but there is an obstruction placed between them. The single target point is only accessible from the left-most skin point. This test demonstrates that the system works by avoiding collisions when obstructions are present.

These test scenarios show that the reachable point algorithm and the algorithm for identifying the best location work as intended. Since finding all reachable points from a given port location is merely an application of the reachable point algorithm, the results demonstrate that this function of the port placement system also works correctly.

More complicated scenes containing a skin model and several enclosed organs were constructed to demonstrate the system's operation. Some of these organ models were derived from real CT/MRI data. Due to the scene's complexity, geometric verification of the results was mathematically intractable. Target areas were selected on one of the models, and the system was used to determine an optimized port location (Figure 9). In addition, multiple port locations were selected manually and scored to verify that the system-selected port location had a better score. During these tests, it was found that the optimized port location for a typical scene can be calculated in only a few minutes on a modern PC.

We also demonstrated the ability of the system to find all possible reachable points from a given port location in a complex scene. As expected, the system avoided points where collisions would occur and indicated only those points that were reachable according to the scoring function. The visualization of these results is shown in Figure 10.

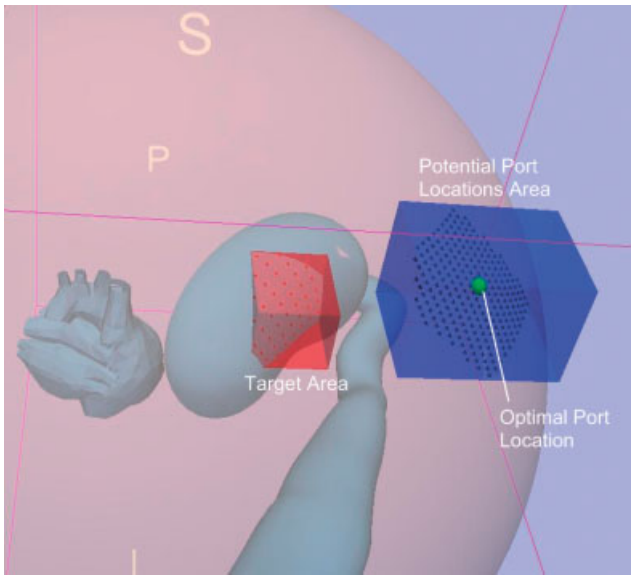

Figure 9. Port placement within the visualization system. The blue box encloses potential port locations, and the green dot indicates the optimal location for use with the enclosed red target area

Discussion

Biosensors and medical robotics used *in vivo* hold the potential to rapidly identify and treat disease. Biosensors have strict physical limitations that make picking a port location a non-trivial task for a human operator. In addition, existing techniques developed for automated port placement were designed for laparoscopic surgical instruments. This work demonstrates a novel automated technique for selecting port locations specifically for biosensor applications. Using existing patient 3D modelling techniques, the system is able to find an optimized location for user-specified targets in a matter of minutes or seconds.

The technique described in this paper does have a few limitations. One limitation is that it assumes that all

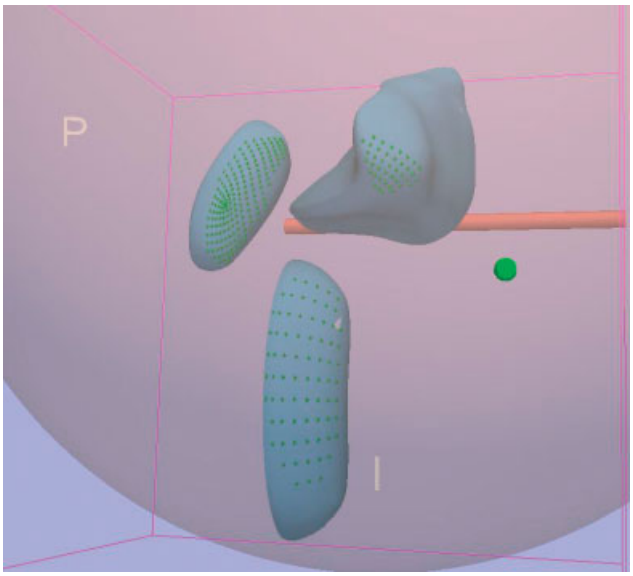

Figure 10. The visualization system, showing all points reachable (green markers) by the biosensor from the manually selected port location (green dot)

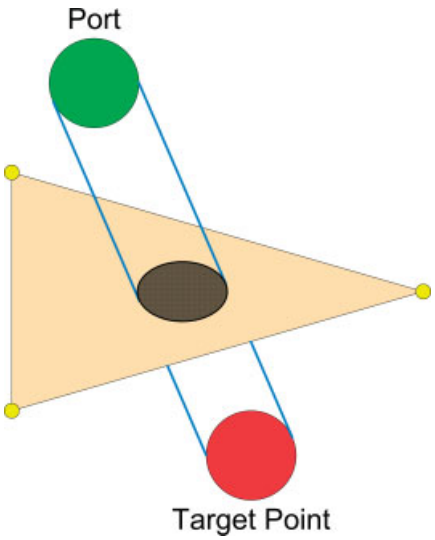

Figure 11. Example of a collision that would be undetected due to wide triangle point spacing. This problem can be prevented with a pre-processing stage

structures are rigid (non-deformable). This limitation is a consequence of the complexity of tissue deformation models. Furthermore, the system also assumes that body structures do not move as a result of manipulation, respiration, etc. Consequently, CT and MRI scans should be taken in the same pose that will be used during the surgery. Additional algorithms would be needed to accommodate tissue deformation and movement. This is an ongoing area of research that could be integrated with the system at a later date.

Another limitation exists within the collision algorithm. There is the possibility of missed collisions with very large triangles in the 3D models. Since this method tests for collisions at the points of a triangle, it is possible for the vector representing the biosensor to pass through the middle of a large triangle (Figure 11). This is possible if each point of the triangle resides outside the radius of the biosensor. In this case, a collision that would obviously occur will go undetected. This potential fault can be eliminated with a pre-processing stage that ensures that the 3D models have none of these triangles. This pre-processing stage would test each triangle in the scene and perform triangle subdivision if any triangle is determined to be too large (25).

Currently, the execution speed of this application is acceptable for the planning process before a surgery. However, there are many possibilities for speed increases. The highly parallel nature of the task makes it a prime candidate for multithreading and parallel processing. Other mechanisms for speed increases include utilizing faster processors and more efficient algorithm implementations. These performance increases may enable near real-time results. If near real-time performance can be achieved, intraoperative medical imaging technology, e.g. 3D ultrasound, could be used to update tissue models and reachable points during a procedure. This possibility would also address the limitation of the algorithms in their assumption of rigid structures.

Currently this work uses a Raman probe as a prototype for the algorithms. However, the system can handle any other biosensor that can be used laparoscopically. To support biosensors of different physical dimensions, modifications can be made to the parameters used in the collision algorithms, such as probe radius and length. Flexible probes can be supported by changing the collision algorithm to a model-based technique. Other types of biosensors (besides Raman spectroscopy probes) can be supported by developing different scoring functions to accommodate their distinct physical data capture characteristics.

For practical applications, it would be best to implement the system with a medical robot. The robot would allow the probe to reach the exact port location and target points within the body. Our research group is currently integrating a portable Raman probe with the Aesop® and Zeus® medical robotic systems (Intuitive Surgical, Sunnyvale, CA, USA). Custom control systems are being developed to enable precise positioning abilities (26).

The next step in this research that will be performed is a human factors study. The study will present a group of users with different virtual scenes, like those described in the Results section. They will be instructed to pick a port location on a 3D skin model that enables the best scans of a target area. Using the system developed in this paper, the users' selections will be compared to the optimized port location. The performance of people on the port placement task will be gauged by using scenes that focus on particular difficulties (irregular surfaces, obstructed target areas, expansive target areas, etc.).

In summary, biosensors have great potential for *in vivo* surgical applications. For example, tissues can be analysed without the need for time-consuming biopsies. In order

to achieve the full potential of a biosensor, it needs to be optimally positioned within the body (e.g. with a robot). A system has been developed for determining optimized port locations for biosensor insertion. This ensures the best coverage of target areas given the limitations of a biosensor. The developed system is an important step towards the goal of utilizing biosensors to improve surgical treatment.

Acknowledgements

This study was supported by Children's Hospital of Michigan. It did not involve human testing, animal testing, or anything else that would raise ethical issues. The authors would like to thank Alex Cao for his contribution to this work.

References

1. Herron D, Marohn M, the Sages–Mira Robotic Surgery Consensus Group. A consensus document on robotic surgery. *Surg Endosc* 2008; **22**(2): 313–325.
2. Prasad SM, Prasad SM, Maniar HS, *et al*. Surgical robotics: impact of motion scaling on task performance. *J Am Coll Surgeons* 2004; **199**(6): 863–868.
3. Wang J. Glucose biosensors: 40 years of advances and challenges. *Electroanalysis* 2001; **13**(12): 983–988.
4. Länge K, Rapp BE, Rapp M. Surface acoustic wave biosensors: a review. *Anal Bioanal Chem* 2008; **391**(5): 1509–1519.
5. Motz JT, Hunter M, Galindo LH, *et al*. Optical fiber probe for biomedical Raman spectroscopy. *Appl Optics* 2004; **43**(3): 542–554.
6. Vo-Dinh T, Cullum B. Biosensors and biochips: advances in biological and medical diagnostics. *Fresenius J Anal Chem* 2000; **366**(6): 540–551.
7. Rabah R, Weber R, Serhatkulu GK, *et al*. Diagnosis of neuroblastoma and ganglioneuroma using Raman spectroscopy. *J Pediatr Surg* 2008; **43**(1): 171–176.
8. Haka AS, Shafer-Peltier KE, Fitzmaurice M, *et al*. Identifying microcalcifications in benign and malignant breast lesions by probing differences in their chemical composition using Raman spectroscopy. *Cancer Res* 2002; **62**(18): 5375–5380.
9. Haka AS, Shafer-Peltier KE, Fitzmaurice M, *et al*. Diagnosing breast cancer by using Raman spectroscopy. *Proc Natl Acad Sci USA* 2005; **102**(35): 12371–12376.
10. Lorincz A, Haddad D, Naik R, *et al*. Raman spectroscopy for neoplastic tissue differentiation: a pilot study. *J Pediatr Surg* 2004; **39**(6): 953–956.
11. Reisner LA, King BW, Klein MD, *et al*. A prototype biosensor-integrated image-guided surgery system. *Int J Med Robotics Comput Assist Surg* 2007; **3**(1): 82–88.
12. Wills H, King B, Reisner L, *et al*. Robotically positioned Raman spectroscopy probe for cancer resection. SAGES Meeting, Philadelphia, PA, 2008.
13. King BW, Reisner LA, Klein MD, *et al*. Registered, sensor-integrated virtual reality for surgical applications. IEEE Virtual Reality Conference, Charlotte, NC, 2007; 277–278.
14. Cannon JW, Stoll JA, Selha SD, *et al*. Port placement planning in robot-assisted coronary artery bypass. *IEEE Trans Robotics Autom* 2003; **19**(5): 912–917.
15. Chiu AM, Dey D, Drangova M, *et al*. 3D image guidance for minimally invasive robotic coronary artery bypass (MIRCAB). *Heart Surg Forum* 2000; **3**(3): 224–231.
16. Selha S, Dupont P, Howe R, *et al*. Dexterity optimization by port placement in robot-assisted minimally invasive surgery. Telemanipulator and Telepresence Technologies VIII, Newton, MA, 2001; 97–104.
17. Tabaie HA, Reinbolt JA, Graper WP, *et al*. Endoscopic coronary artery bypass graft (ECABG) procedure with robotic assistance. *Heart Surg Forum* 1999; **2**(4): 310–317.
18. Trejos AL, Patel RV, Ross I, *et al*. Optimizing port placement for robot-assisted minimally invasive cardiac surgery. *Int J Med Robotics Comput Assist Surg* 2007; **3**(4): 355–364.
19. Navab N, Traub J, Sielhorst T, *et al*. Action- and workflow-driven augmented reality for computer-aided medical procedures. *IEEE Comput Graphics Applic* 2007; **27**(5): 10–14.
20. Traub J, Feuerstein M, Bauer M, *et al*. *Augmented Reality for Port Placement and Navigation in Robotically Assisted Minimally Invasive Cardiovascular Surgery*. Computer Assisted Radiology and Surgery Conference (CARS 2004), Chicago, USA. Elsevier: Amsterdam, 2004; 735–740.
21. Motz JT, Gandhi SJ, Scepanovic OR, *et al*. Real-time Raman system for *in vivo* disease diagnosis. *J Biomed Optics* 2005; **10**(3): 031113.
22. Haka AS, Volynskaya Z, Gardecki JA, *et al*. *In vivo* margin assessment during partial mastectomy breast surgery using Raman spectroscopy. *Cancer Res* 2006; **66**(6): 3317–3322.
23. Bakker Schut TC, Witjes MJH, Sterenborg HJCM, *et al*. *In vivo* detection of dysplastic tissue by Raman spectroscopy. *Anal Chem* 2000; **72**(24): 6010–6018.
24. Gering DT, Nabavi A, Kikinis R, *et al*. An integrated visualization system for surgical planning and guidance using image fusion and an open MR. *J Magnet Reson Imaging* 2001; **13**(6): 967–975.
25. Warren J, Schaefer S. A factored approach to subdivision surfaces. *IEEE Comput Graphics Applic* 2004; **24**(3): 74–81.
26. Daluja S, Golenberg L, Cao A, *et al*. An integrated movement capture and control platform applied towards autonomous movements of surgical robots. Medicine Meets Virtual Reality 17, Long Beach, CA, 19–22 January 2009.